Contribution from the Departments of Chemistry and Physics, Northwestern University, Evanston, Illinois 60201, and the Physics Division, Argonne National Laboratory, Argonne, Illinois 60439

Xα Calculations and Spectroscopic Studies of Triruthenium and Triosmium Dodecacarbonyls[1]

BERNARD DELLEY,[2a] MARK C. MANNING,[2b] D. E. ELLIS,*[2b] JOSEPH BERKOWITZ,[2c] and WILLIAM C. TROGLER*[2b]

Received August 6, 1981

Nonempirical calculations of the Xα type are reported for $Ru_3(CO)_{12}$ and $Os_3(CO)_{12}$. Two procedures were used to model the molecular charge density for calculating the self-consistent potential: an approximate self-consistent charge scheme and the more rigorous superposition of multipolar densities. This latter type of procedure accurately calculates the splitting of occupied d orbitals in $Ru_3(CO)_{12}$ and $Os_3(CO)_{12}$. Centrally directed metal–metal σ- and π-bonding orbitals are occupied as well as their antibonding counterparts. Stability of the latter levels results from metal–carbon monoxide π bonding. A filled degenerate cyclopropane-like edge-bonding orbital furnishes four bonding electrons to the cluster framework. Difference electron density maps aid the analysis of the two lowest energy electronic transitions. The dipole-allowed transition ($15e' \rightarrow 6a_2'$) should be strongly metal–metal antibonding, and the dipole-forbidden HOMO → LUMO excitation ($10a_1' \rightarrow 6a_2'$) is predominantly transition-metal–CO antibonding. Raman spectra for $Ru_3(CO)_{12}$ exhibit resonance enhancement of *both* the 185 (a_1') and 130-cm^{-1} (e') Ru–Ru stretching vibrations. This behavior confirms the predicted antibonding nature of the lowest allowed transition and suggests a Jahn–Teller distortion in the excited state or *B*-term scattering. Spectrophotometric titrations show the metal center in $Os_3(CO)_{12}$ to be approximately 5 times more basic toward the proton than that in $Ru_3(CO)_{12}$.

Introduction

Interest in spectroscopic and bonding properties of the group 8 trinuclear carbonyl cluster complexes originated in 1951.[3a] At that time an atomic-like 4s → 4p transition seemed the most probable assignment for the 608-nm absorption band in $Fe_3(CO)_{12}$. During the 1960s the structures of $Fe_3(CO)_{12}$,[3b] $Ru_3(CO)_{12}$,[4] and $Os_3(CO)_{12}$[5] were elucidated by crystallographic and spectroscopic analyses. Yawney and Stone, as well as Chini,[6] suggested that the colors of these clusters result from electronic transitions that involve metal–metal bonding electrons. As experimental studies progressed, topological orbital[7] (or electron-counting) theoretical models emerged. Pauling[8] later applied simple valence bond theory to these systems, and the bond number calculated for $Os_3(CO)_{12}$ suggested that two single bonds resonate among three positions of the metal framework. Korol'kov and Miessner[9] performed a pioneering orbital calculation of $Os_3(CO)_{12}$ that employed the extended Hückel molecular orbital method. Similar calculations have recently been reported for $Fe_3(CO)_{12}$[10] and $Ru_3(CO)_{12}$.[11] The complete neglect of differential overlap approximation has been implemented[12] in a calculation of ionization potentials (IP's) for $Ru_3(CO)_{12}$. Although the various molecular orbital models agree in some qualitative aspects, no satisfactory quantitative descriptions are presently available.[13] The solid-state[14] and vapor-phase[12,15] photoelectron spectra of $Ru_3(CO)_{12}$ and $Os_3(CO)_{12}$ were reported during the course of our study. Two different MO orderings[12,15] were proposed for $Ru_3(CO)_{12}$ on the basis of the experimental data and semiempirical orbital models.

The lowest electronic excited states in $Fe_3(CO)_{12}$, $Ru_3(CO)_{12}$, $Os_3(CO)_{12}$, and related complexes were probed with magnetic circular dichroism and polarized single-crystal spectroscopic techniques.[11] In $Ru_3(CO)_{12}$ and $Os_3(CO)_{12}$ the lowest allowed electronic transition was degenerate and thought to be metal bonding to metal antibonding in character. One-electron reduction of these compounds leads to irreversible fragmentation,[16] and the reduction potential correlates with the LUMO energy. Excited-state electronic properties are also pertinent to the enigmatic photochemical reactivities of these systems. In some cases photofragmentation of $Fe_3(CO)_{12}$, $Ru_3(CO)_{12}$, and $Os_3(CO)_{12}$ has been reported to be the major photochemical pathway,[17] while in other instances the cluster framework remains intact and CO is substituted.[18]

Triruthenium and triosmium dodecacarbonyls constitute the simplest examples of metal carbonyl cluster complexes. Their high symmetry (Figure 1) makes them attractive choices for fundamental spectroscopic and theoretical study. Bonding properties of a triangular array of metal atoms also relate to the electronic structures of larger clusters.[19] For example, octahedral clusters are comprised of eight triangular faces, and the electronic properties of trimeric cluster complexes might be of use in a fragment analysis.[20] Trinuclear metal carbonyl

(1) Part 2 in the series "Spectroscopic and Theoretical Studies of Metal Cluster Complexes".
(2) (a) Department of Physics. (b) Department of Chemistry. (c) Argonne National Laboratory.
(3) (a) Sheline, R. K. *J. Am. Chem. Soc.* **1951**, *73*, 1615–1618. (b) Wei, C. H.; Dahl, L. F. *Ibid.* **1969**, *91*, 1351–1361 and references therein.
(4) Mason, R.; Rae, A. I. M. *J. Chem. Soc. A* **1968**, 778–779.
(5) Dahl, L. F.; Corey, E. R. *Inorg. Chem.* **1962**, *1*, 521–526.
(6) Yawney, D. B. W.; Stone, F. G. A. *J. Chem. Soc. A* **1969**, 502–506. Chini, P. *Pure Appl. Chem.* **1970**, *23*, 489–503.
(7) Brown, D. A. *J. Inorg. Nucl. Chem.* **1958**, *5*, 289–291. Kettle, S. F. A. *J. Chem. Soc. A* **1966**, 1013–1014.
(8) Pauling, L. *Proc. Natl. Acad. Sci. U.S.A.* **1976**, *73*, 4290–4293.
(9) Korol'kov, D. V.; Miessner, H. *Z. Phys. Chem. (Leipzig)* **1973**, *253*, 25–32; *Vestn. Leningr. Univ., Fiz. Khim.* **1974**, *4*, 74–83.
(10) Schilling, B. E. R.; Hoffmann, R. *J. Am. Chem. Soc.* **1979**, *101*, 3456–3467.
(11) Tyler, D. R.; Levenson, R. A.; Gray, H. B. *J. Am. Chem. Soc.* **1978**, *100*, 7888–7893.
(12) Ajo, D.; Granozzi, G.; Tondello, E.; Fragala, I. *Inorg. Chim. Acta* **1979**, *37*, 191–193.
(13) For a review of the electronic structures of metal cluster complexes, see: Manning, M. C.; Trogler, W. C. *Coord. Chem. Rev.* **1981**, *38*, 89–138.
(14) Plummer, E. W.; Salaneck, W. R.; Miller, J. S. *Phys. Rev. B: Condens. Matter* **1978**, *18*, 1673–1701.
(15) Green, J. C.; Seddon, E. A.; Mingos, D. M. P. *J. Chem. Soc., Chem. Commun.* **1979**, 94–95; *J. Organomet. Chem.* **1980**, *185*, C20–24; *Inorg. Chem.* **1981**, *20*, 2595–2602.
(16) Bond, A. M.; Dawson, P. A.; Peake, B. M.; Robinson, B. H.; Simpson, J. *Inorg. Chem.* **1977**, *16*, 2199–2206.
(17) Knox, S. A. R.; Stone, F. G. A. *J. Chem. Soc. A* **1969**, 2559–2565; **1970**, 3147–3153; **1971**, 2874–2880. Brookes, A.; Knox, S. A. R.; Stone, F. G. A. *Ibid.* **1971**, 3468–3471. Cotton, F. A.; Deeming, A. J.; Justy, P. L.; Sullah, S.; Domingos, A. J. P.; Johnson, B. F. G.; Lewis, J. *J. Am. Chem. Soc.* **1971**, *93*, 4624–4626. Johnson, B. F. G.; Lewis, J.; Twigg, M. V. *J. Organomet. Chem.* **1974**, *67*, C75–76. Zobl-Ruh, S.; von Philipsborn, W.; *Helv. Chim. Acta* **1980**, *63*, 773–779.
(18) Cullen, W. R.; Harbourne, D. A.; Liengme, B. V.; Sams, J. R. *J. Am. Chem. Soc.* **1968**, *90*, 3293–3295; *Inorg. Chem.* **1970**, *9*, 702–710. Cullen, W. R.; Harbourne, D. A. *Ibid.* **1970**, *9*, 1839–1843. Roberts, P. J.; Trotter, J. *J. Chem. Soc. A* **1971**, 1479–1482. Burkhardt, E. W.; Geoffroy, G. L. *J. Organomet. Chem.* **1980**, *198*, 179–188. Tyler, D. R.; Altobelli, M.; Gray, H. B. *J. Am. Chem. Soc.* **1980**, *102*, 3022–3024.
(19) King, R. B. *J. Am. Chem. Soc.* **1972**, *94*, 95–103. Chini, P.; Longoni, G.; Albano, V. G. *Adv. Organomet. Chem.* **1976**, *14*, 285–344.
(20) Elian, M.; Hoffmann, R. *Inorg. Chem.* **1975**, *14*, 1058–1076. Elian, M.; Maynard, M. L.; Chen, D.; Mingos, D. M. P.; Hoffmann, R. *Ibid.* **1976**, *15*, 1148–1155.

0020-1669/82/1321-2247$01.25/0

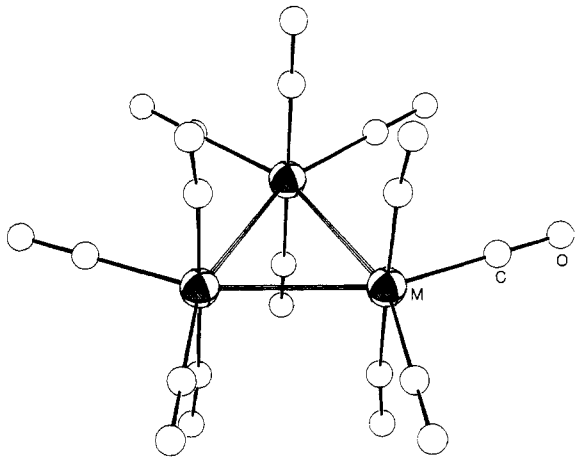

Figure 1. Molecular structure adopted by $Ru_3(CO)_{12}$ and $Os_3(CO)_{12}$.

complexes have attracted recent attention due to their catalytic activity[21,22] and their relevance to surface catalysis.[23]

Experimental Section

The photoelectron spectrometer, which consists of a cylindrical-mirror electron-energy analyzer, has been described previously.[24] A noninductively wound resistance-heated Pt furnace (containing solid $M_3(CO)_{12}$) provided a molecular beam for photoionization measurements. The Raman apparatus consisted of a Spex 1401 double monochromator, an argon ion Spectra-Physics laser, and detection electronics. Samples were concentrated CH_2Cl_2 or THF solutions in 5-mm tubes, which were rotated to eliminate local sample heating. A back-scattering geometry was adopted. At the laser power levels employed cluster decomposition was not a significant problem. Spectra "on resonance" only evidence bands already observed "off resonance", and a series of Raman intensity measurements could be recorded and then reproduced (±15%) with the same sample.

Preparation of $Os_3(CO)_{10}[P(C_6H_5)_2(C_{10}H_{19})]_2$. A Schlenk flask was charged with 0.30 g (0.33 mmol) of $Os_3(CO)_{12}$ and 0.34 g (1.048 mmol) of diphenylneomenthylphosphine, $P(C_6H_5)_2(C_{10}H_{19})$. Approximately 25 mL of toluene was distilled into the flask under nitrogen. The solution was refluxed for 6 h (nitrogen atmosphere), during which time it turned from yellow to dark red. Removal of the solvent in vacuo left a red oil. The oil was dissolved in a mixture of petroleum ether and toluene (6:4, v/v) and eluted on an alumina column with this solvent. Four bands corresponding to $Os_3(CO)_{12}$ and its mono-, bis-, and tris(phosphine) complexes, respectively, eluted from the column, and the major product was the orange bis(phosphine) cluster. This complex dissolves in hydrocarbon solvents as well as in polar solvents such as THF and acetone. The air-stable solid was purified by precipitation from acetone upon careful addition of water; yield 0.28 g (0.187 mmol), 56.4%. Anal. Calcd for $Os_3C_{54}H_{58}O_{10}P_2$: C, 43.24; H, 3.87. Found: C, 43.7; H, 3.8. Carbonyl stretching bands at 2090 mw, 2034 ms, 2018 m, 2003 vs, 1968 m, and 1948 mw cm^{-1} closely approximate those reported[25] for the disubtituted cluster complex $Os_3(CO)_{10}(P(C_6H_5)_3)_2$ (at 2085 mw, 2030 s, 2012 m, 1998 s, 1969 m, and 1951 mw cm^{-1} in CCl_4 solvent) and suggest a similar structure. The ^{31}P NMR spectrum exhibited singlets of approximately equal intensity at −1.8 and +1.8 ppm (85% H_3PO_4 external standard).

Theoretical Methods. Theoretical electronic structure calculations adopted the discrete variational[26] (DV) Xα approach. Two procedures were employed to approximate the molecular electron density used to generate the self-consistent potential. In the self-consistent charge (SCC) approximation[27] the molecular charge density is represented as a superposition of spherical atomic orbital densities, and the latter coefficients are determined by a weighted population analysis. For the multipolar potential (MP) calculations the molecular charge density was expressed as a superposition of multipolar densities. In addition to atomic radial densities, the expansion basis consists of localized radial functions multiplied by spherical harmonics, attached to nuclear sites. A kind of histogram representation for the radial densities $\rho_{\nu(LM)}$ is built up by a least-squares procedure, which can lead to an essentially perfect fit to the molecular density.[28] Sufficient flexibility was obtained for the present case with seven radial degrees of freedom and $l = 0, 1$ spherical harmonics. Numerical atomic orbitals (through 5p on Ru and through 6p on Os) were employed as basis functions. Due to the size of the system a "frozen-core" approximation was necessary for all $Os_3(CO)_{12}$ calculations and for the MP calculation of $Ru_3(CO)_{12}$. The valence orbitals were explicitly orthogonalized against numerical atomic core wave functions, and the secular equation was solved in the reduced valence-function space. No significant changes were found due to this procedure, by comparison with fully variational results for the Ru system. Experimental geometries[29] of $Ru_3(CO)_{12}$ and $Os_3(CO)_{12}$ were idealized to D_{3h} symmetry for use in the calculations.

It is well-known[30] that the statistical total energy does *not* represent the expectation value of an *n*-electron wavefunction but represents an ensemble average over single-particle states. Local density functional theory[30] generates a set of orthogonal single-particle orbitals based upon a particular set of Fermi–Dirac occupation numbers. Single-particle excitation energies (as well as ionization potentials) are calculated by treating the variation of E_{tot} with occupation number; again no single *n*-electron state is invoked. For treating multiplet splittings, where electron coupling is explicitly required, it is conventional to build a multideterminant model constructed from the local density orbitals. This approach to multiplet effects has been shown to be quite successful in molecules[31] as well as in atomic systems.[30] This elaboration of local density single-particle theory is not necessary for our present objectives, the description of general features of UPS binding energies and one-electron optical transitions. For detailed interpretation of d^n multiplet structure and spin–orbit splittings, we acknowledge that the many-electron approach will be needed.

Results and Discussion

In previous studies,[32,33] we explored the utility of the SCC–DV–Xα method for facilitating the assignment of electronic and photoelectron spectra of inorganic complexes. Because of the unusual strength (and electronic asymmetry) of the CO bond, the approximation of the molecular electron density as a (SCC) superposition of spherical charge densities is questionable.[28] A least-squares procedure[28] has been developed to fit more exactly the molecular electron density in the potential calculations, and computations for small molecules[28] (e.g, CO) demonstrate the accuracy of this approach. Hereafter, we denote predictions from such a computation as the "multipolar potential" (MP–DV–Xα) result. Two Xα

(21) Muetterties, E. L.; Demitras, G. C. *J. Am. Chem. Soc.* **1977**, *99*, 2796–2797. Muetterties, E. L.; Beier, B. F.; Thomas, M. G. *Ibid.* **1976**, *98*, 1296–1297. Ungermann, C.; Landis, V.; Moya, S. A.; Cohen, H.; Walker, H.; Pearson, R. G.; Ford, P. C. *Ibid.* **1979**, *101*, 5922–5929. Watson, P. L.; Schrader, G. L. *J. Mol. Catal.* **1980**, *9*, 129–138.
(22) Asinger, F.; Fell, B.; Schrage, K. *Chem. Ber.* **1964**, *98*, 372–386. Carr, M. D.; Kane, V. V. Whiting, M. C. *Proc. Chem. Soc., London* **1964**, 408–409. Austin, R. G.; Paonessa, R. S.; Giordano, P. J.; Wrighton, M. S. *Adv. Chem. Ser.* **1978**, *No. 168*, 189–214. Graff, J. L.; Sanner, R. D.; Wrighton, M. S. *J. Am. Chem. Soc.* **1979**, *101*, 273–275.
(23) Kaesz, H. D. *Chem. Br.* **1973**, *9*, 344–352. Ugo, R. *Catal. Rev.-Sci. Eng.* **1975**, *11*, 225–297. Muetterties, E. L. *Science (Washington D.C.)* **1977**, *196*, 839–848. Hemminger, J. C.; Muetterties, E. L.; Somorjai, G. *J. Am. Chem. Soc.* **1979**, *101*, 62–67.
(24) Berkowitz, J. *J. Chem. Phys.* **1972**, *56*, 2766–2774.
(25) Bradford, C. W.; van Bronswijk, W.; Clark, R. J. H.; Nyholm, R. S. *J. Chem. Soc. A* **1970**, 2889–2899. For the structure of disubstituted clusters, see: Johnson, B. F. G.; Lewis, J.; Reichardt, B. E.; Schorpp, K. T. *J. Chem. Soc., Dalton Trans.* **1976**, 1403–1406.
(26) Ellis, D. E.; Painter, G. S. *Phys. Rev. B.: Solid State* **1970**, *2*, 2887–2898. Baerends, E. J.; Ellis, D. E.; Ros, P. *Chem. Phys.* **1973**, *2*, 41–51.
(27) Ellis, D. E.; Rosen, A.; Adachi, H.; Averill, F. W. *J. Chem. Phys.* **1976**, *65*, 3629–3634.
(28) Delley, B.; Ellis, D. E. *J. Chem. Phys.* **1982**, *76*, 1949–1960.
(29) Churchill, M. R.; Hollander, F. J.; Hutchinson, J. P. *Inorg. Chem.* **1977**, *16*, 2655–2659. Churchill, M. R.; DeBoer, B. G. *Ibid.* 878–884.
(30) Slater, J. C. "The Self-Consistent Field for Molecules and Solids"; McGraw-Hill: New York, 1974.
(31) Ziegler, T. Ph.D. Thesis, University of Calgary, 1978.
(32) Trogler, W. C.; Ellis, D. E.; Berkowitz, J. *J. Am. Chem. Soc.* **1979**, *101*, 5896–5901.
(33) Trogler, W. C.; Desjardins, S. R.; Solomon, E. I. *Inorg. Chem.* **1979**, *18*, 2131–2136. Trogler, W. C.; Johnson, C. E.; Ellis, D. E. *Ibid.* **1981**, *20*, 980–986. Gross, M. E.; Trogler, W. C.; Ibers, J. A. *J. Am. Chem. Soc.* **1981**, *103*, 192–193.

Table I. Atomic Character[a] of the Frontier Orbitals from the Multipolar Potential DV-Xα Calculation of $Ru_3(CO)_{12}$[b]

orbital	energy, eV	% Ru 5s	% Ru 5p	% Ru 4d	% axial CO s (p)	% equatorial CO s (p)	major Ru_3 and $(CO)_{12}$ contribns
				Unoccupied Orbitals			
17e′	−4.02	2	1	8	4 (72)	3 (9)	CO π*
$7a_2''$	−4.14		1	10	3 (3)	(83)	Ru π_c, CO π*
$11a_1''$	−4.33	8	9	7	(38)	2 (35)	CO π*
16e′	−4.55			7	1 (67)	6 (17)	CO π*
$6a_2'$	−4.91		8	26	(31)	10 (25)	Ru σ_{cp}*, CO π*
				Occupied Orbitals			
$10a_1'$	−7.54	5	29	17	(32)	3 (14)	Ru p_{σ_c}, σ_1, CO π*
15e′	−7.60		20	43	(11)	12 (13)	Ru σ_{cp}, $p_{\sigma_{cp}}$, CO π*
14e′	−8.57			74	(1)	1 (23)	Ru σ_c*, CO π*
9e″	−8.72			74	(16)	(8)	Ru π_c*, π_1, CO π*
$3a_1''$	−9.01			75	(13)	(12)	Ru π_1, CO π*
8e″	−9.56			74	(14)	(10)	Ru π_1, CO π*
$6a_2''$	−9.76			72	1 (19)	(7)	Ru π_c, CO π*
$9a_1'$	−9.88	2	1	83	(2)	(11)	Ru σ_c, CO π*
7e″	−12.00		2		43 (50)	(5)	CO σ
$5a_2''$	−12.45		6		37 (50)	(6)	CO σ

[a] Values are rounded off to the nearest percent. A weighted Mulliken type population analysis of the density matrix was used to generate these values. [b] A total of 22 CO 5σ and CO 1π orbitals are found between −13 and −14.4 eV. The 4σ CO-based levels 2e″, $2a_2''$, $2a_2'$, 6e′, 5e′, $4a_1'$, 4e′, and $3a_1'$ lie between −15.06 and −16.84 eV. The 3σ orbitals (oxygen lone pairs) $2a_1'$, $1a_1'$, 3e′, 2e′, $1a_2'$, 1e′, $1a_2''$, and 1e″ are between −32.51 and −32.72 eV.

Table II. Band Maxima[a] in the He I Photoelectron Spectra of $Ru_3(CO)_{12}$ and $Os_3(CO)_{12}$

band	IP, eV $Ru_3(CO)_{12}$	IP, eV $Os_3(CO)_{12}$	assignt
A	7.9	7.88	10a′
		8.29	15e′
B		8.49	
C	9.2	9.63	14e′, 9e″, $3a_1''$
D	10.2	10.44	8e″, $6a_2''$, $9a_1''$
E	13.2	13.52	7e″
F	14.8 br	15.08 br	various CO-based IP's

[a] The $Ru_3(CO)_{12}$ data were only reproducible to ±0.2 eV because of the deleterious effect of solid deposited near the ionization region and the high background due to free CO from sample decomposition in the oven; the $Os_3(CO)_{12}$ energies were much better determined and found reproducible to ±0.05 eV.

calculations of $Ru_3(CO)_{12}$ were performed. One included all electrons and adopted the SCC approximation.[27] The second employed a frozen core and utilized the MP for all valence electrons. Both the SCC and MP $Os_3(CO)_{12}$ calculations used the frozen-core approximation. All four calculations produced qualitatively similar energy level diagrams and wave functions. Table I contains the frontier orbital wave functions for the MP study of $Ru_3(CO)_{12}$. Supplementary Table I collects eigenvalues of the other calculations. Quantitative differences between the various methods are best illustrated by calculated values of experimental properties.

Photoelectron Spectra and Theory. The He I photoelectron spectra of $Ru_3(CO)_{12}$ and $Os_3(CO)_{12}$ provide a clean separation of the occupied metal- and CO-based valence orbitals. Predominantly metal-localized orbitals lie between 7.5 and 10.5 eV. The spectra listed in Table II agree well with those of the previous experimental studies.[12,15] Electrons derived from the 5σ and 1π orbitals of carbon monoxide occur at energies above 13.2 eV. The spectra of $Ru_3(CO)_{12}$ and $Os_3(CO)_{12}$ are very similar except for more extensive splitting of the d band in the latter complex.

Calculated ionization potentials (IP's) for $Ru_3(CO)_{12}$ and $Os_3(CO)_{12}$ from all four calculations are listed in supplementary Table II. Theoretical IP's are *uniformly* overestimated by some 1.7–2.7 eV, depending on the type of calculation. Multipolar potential results are better than SCC values; however, both theories inadequately predict absolute ionization

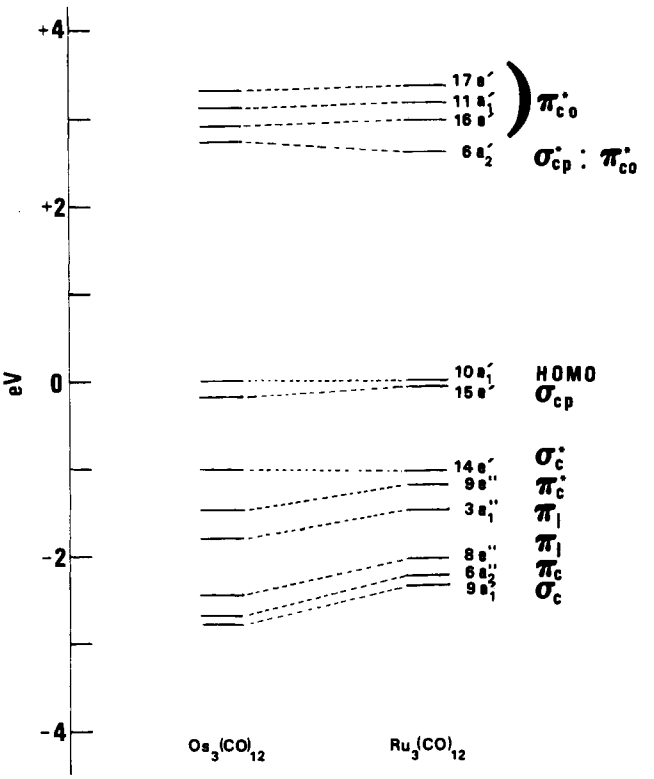

Figure 2. Comparison of frontier orbital splittings in the multipolar potential DV–Xα calculations for $Ru_3(CO)_{12}$ and $Os_3(CO)_{12}$. The $10a_1'$ HOMO level has been adjusted to 0 eV for comparative purposes. Predominant orbital character is given by symbols at the right, which are defined in Figure 3.

energies. The theories do accurately account for relative orbital energies (Figure 2). For example, the valence d-orbital ionization energies (bands A–D, Table II) are split by 2.3 and 2.56 eV in $Ru_3(CO)_{12}$ and $Os_3(CO)_{12}$, respectively. The SCC (MP) results predict 2.4 (2.3) eV for $Ru_3(CO)_{12}$. Similar calculated values for $Os_3(CO)_{12}$ are 2.6 (2.8) eV. The second unambiguous spectral feature is the energy gap between the d band and the CO localized IP's. These gaps are 3.0 and 3.08 eV for $Ru_3(CO)_{12}$ and $Os_3(CO)_{12}$, respectively. Calculated SCC (MP) gap energies for $Ru_3(CO)_{12}$ and $Os_3(CO)_{12}$ are 2.5 (2.3) and 1.3 (1.7) eV. In this instance, the full potential

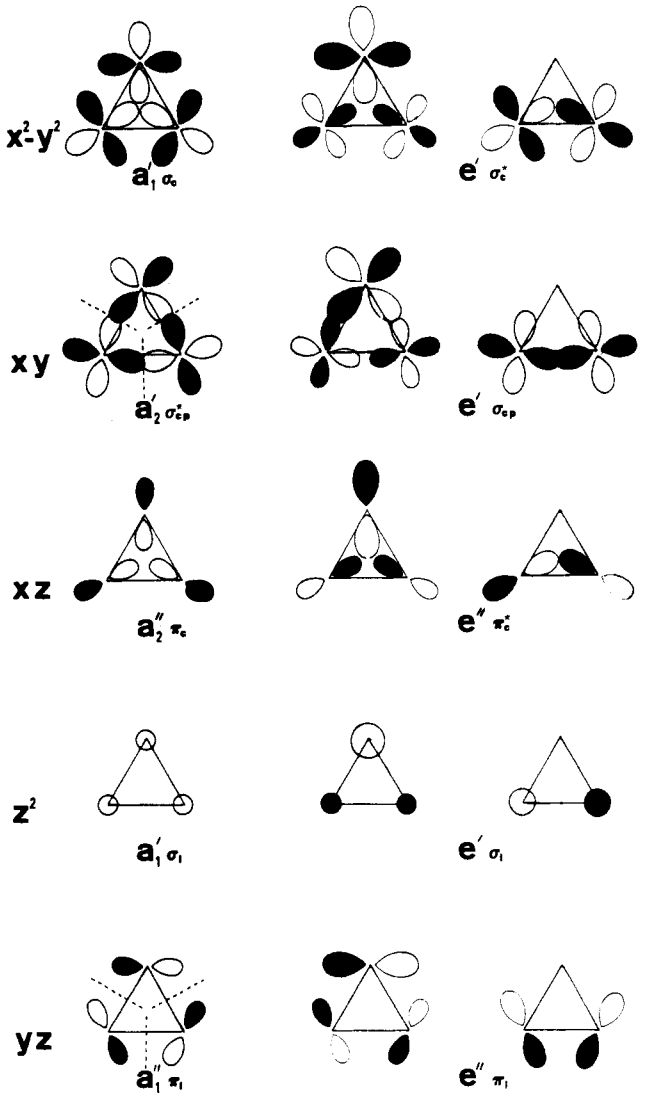

Figure 3. Symmetry combinations of the metal d orbitals. Centrally directed metal–metal bonding orbitals are denoted with the subscript c and edge-bonding orbitals by the subscript cp. Orbitals that chiefly interact with the CO ligands possess a subscript l. In these figures the z axis conicides with the C_3 symmetry axis.

result is 0.7 eV in error for $Ru_3(CO)_{12}$. The discrepancy increases in the osmium complex. Theoretical calculations reported here are nonrelativistic. In view of the significant d-level shifts and indirect screening effects found in relativeistic studies of atoms and smaller molecules,[34] it would be desirable to carry out Dirac–Slater self-consistent studies on both ruthenium and osmium complexes.

The calculations suggest the specific assignments for the ionization potentials listed in Table II. These assignments are consistent with the integrated relative band intensities reported previously.[15] The ratio 1:2.9 of the (A + B):(C + D) band areas lies close to that of 1:3 expected on the basis of the assignments in Table II. Note that the Ru and Os valence electrons are, on the average, more bound than those in atomic Ru (appearance potential AP = 7.16 ± 0.07 eV) or Os (AP = 8.15 ± 0.09 eV).[35] This added stability would be an expected consequence of metal–CO back-bonding and metal–metal bonding.

Our computational results are grossly similar to the earlier qualitative MO schemes[9,10,11,15] but suggest a smaller $10a_1'$–$15e'$ orbital splitting and a greater d-band splitting than that

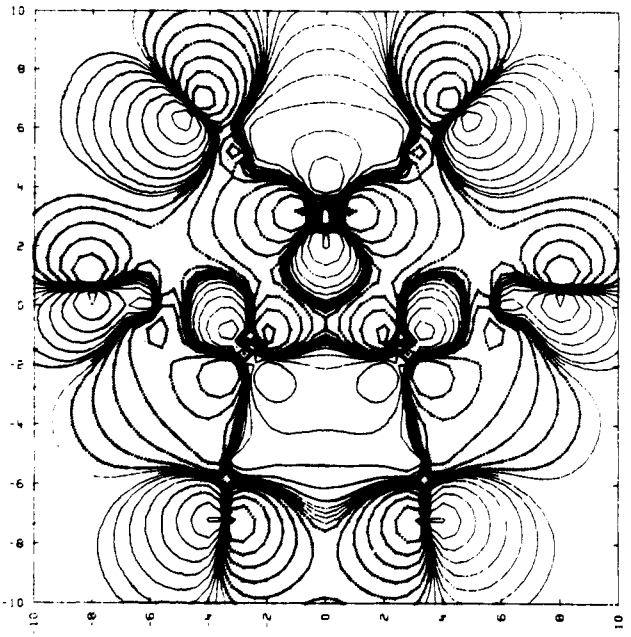

Figure 4. Contour plot of the $14e'$ (σ_c^*) orbital in $Ru_3(CO)_{12}$. The section is in the Ru_3 plane, and the lowest contour level is 0.001 e/a_0^3 with subsequent contours double the previous value. In these and subsequent plots the triangular Ru_3 array stands out, as well as the oxygen atoms on the periphery. Carbon atoms (which are less obvious) may then be visualized by interpolation.

in previous studies. Photoelectron spectroscopic data directly establishes the small (0.3 eV) $10a_1$–$15e'$ orbital splitting and the large d-band splitting. Qualitative differences between the Hückel and Xα orbitals will now be examined.

Nature of the Bonding Orbitals. In Figure 3 the d orbitals in $Ru_3(CO)_{12}$ are classified according to their bonding character. Orbitals that participate in cluster (i.e., directed to the center of the cluster) bonding are denoted with the subscript c, and the subscript cp denotes orbitals that overlap along the edges of the triangle. Those d orbitals that overlap poorly with each other but are directed toward the ligands are represented with a subscript l. Dominant contributions to the frontier molecular orbitals provide a simple interpretation of Figure 2. The most stable metal-localized orbitals are those that engage in metal–metal σ_c and π_c bonding and those that π bond with CO (i.e., π_l). It should be remembered that the σ_c and π_c orbitals gain enhanced stability due to the CO ligands. This stability may be attributed to direct π bonding[36] with CO and to the partial positive charge acquired by the metal (a population analysis in supplementary Table III indicates a 1.1+ net charge on Ru). Figure 4 illustrates the extensive Ru–CO π bonding in σ_c^*. Therefore, the σ_c^*, and for similar reasons the π_c^*, levels become occupied, and the net metal–metal cluster bonding cancels. Similar ligand stabilization of metal–metal antibonding orbitals in electron-rich clusters occurs in dimeric complexes.[37a] Net metal–metal

(34) Rosen, A.; Ellis, D. E. *J. Chem. Phys.* **1975**, *62*, 3039–3048.
(35) Rauh, E. G.; Ackermann, R. J. *J. Chem. Phys.* **1979**, *70*, 1004–1007.

(36) Descriptions of metal–CO π back-bonding may depend on the method of analysis of the electron density distribution as in: Beach, N. A.; Gray, H. B. *J. Am. Chem. Soc.* **1968**, *90*, 5713–5721. Hillier, I. H.; Saunders, V. R. *Mol. Phys.* **1971**, *22*, 1025–1034. Baerends, E. J.; Ros, P. *Ibid.* **1975**, *30*, 1735–1747. Caulton, K. G.; Fenske, R. F. *Inorg. Chem.* **1968**, *7*, 1273–1284. Johnson, J. B.; Klemperer, W. G. *J. Am. Chem. Soc.* **1977**, *99*, 7132–7137. Bursten, B. E.; Freier, D. G.; Fenske, R. F. *Inorg. Chem.* **1980**, *19*, 1810–1811. Sherwood, D. E.; Hall, M. B. *Ibid.* **1980**, *19*, 1805–1809. Our results provide evidence for significant back-bonding in the $M_3(CO)_{12}$ complexes.

(37) (a) Trogler, W. C. *J. Chem. Educ.* **1980**, *57*, 424–427. (b) In a private communication, Professor Hoffmann has informed us that the $10a_1'$ orbital in ref 10 actually contains about 70% carbon monoxide character. The qualitative sketches of this orbital in ref 10 and 15 are therefore oversimplified, and the conclusion that the HOMO $10a_1'$ level be assigned to a predominantly cluster bonding orbital[15] is not correct.

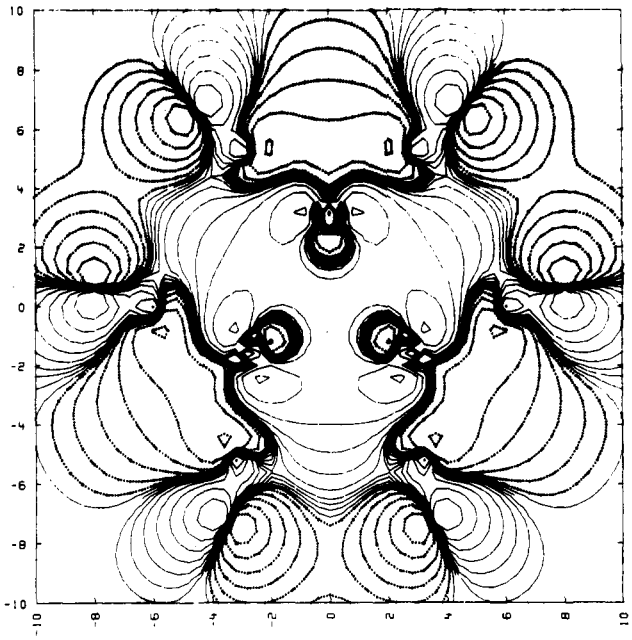

Figure 5. Contour plot of the $10a_1'$ orbital (plot parameters as in Figure 4).

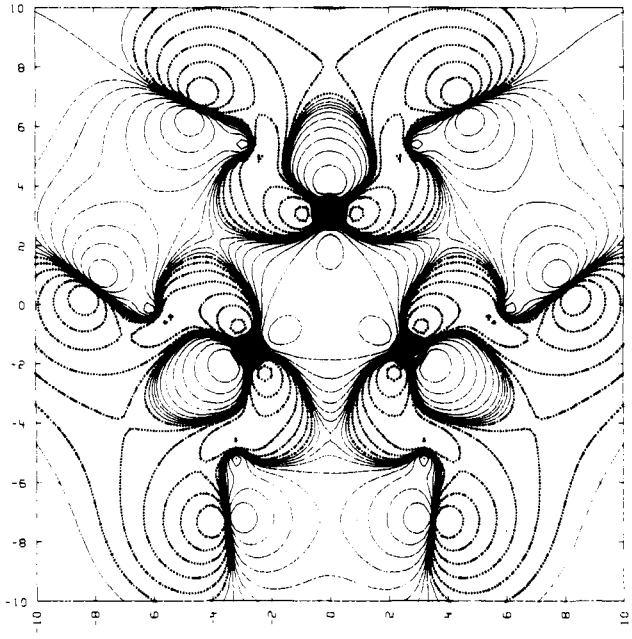

Figure 6. Contour plot of the $9a_1'$ orbital (plot parameters as in Figure 4).

bonding in $Ru_3(CO)_{12}$ and $Os_3(CO)_{12}$ chiefly arises from the $15e'$ (σ_{cp}) orbital. The four-electron bonding corresponds to Pauling's valence bond description[8] of two edge bonds resonating among three triangular positions.

Some metal–metal bonding appears in $10a_1'$ (Figure 5), which consists of 29% σ_c character from *metal p orbitals* and a small (14%) σ_1 d contribution. Of equal import are the 14% equatorial and 32% axial CO(π^*) components. A tilting of the CO-based 2p orbitals (Figure 5) toward the back lobes of the centrally directed Ru 5p orbitals indicates appreciable metal–CO bonding in this level. Although a previous Hückel study[15] likened the $10a_1'$ and $15e'$ orbitals to the Walsh-like bonding orbitals of cyclopropane, we find $9a_1'$ to better represent the d-orbital σ_c bond (Figure 6). Apparently Green et al.[15] did not realize the dominant CO character of the $10a_1'$ orbital predicted by the Hückel calculation.[37b] The $10a_1'$ orbital is best described as a covalent mixture of Ru–CO π bonding, σ_c bonding exclusively due to Ru 5p character, and Ru–CO σ antibonding. In this picture, $9a_1'$ and $15e'$ are the d-orbital analogues of cyclopropane. The relatively high placement of the metal–metal bonding $15e'$ (σ_{cp}) orbital stems from its σ-antibonding interaction with equatorial carbon monoxide ligands. As expected the σ_{cp}^* orbital is not occupied, nor are the σ_1 d orbitals.

Table III. Calculated and Experimental Electronic Transition Energies (eV)

molecule	electronic transition	dipole allowed	calcd energy SCC	calcd energy MP	exptl[b] energy
$Ru_3(CO)_{12}$	$10a_1' \rightarrow 6a_2'$	no		2.70[a]	not obsd
$Ru_3(CO)_{12}$	$15e' \rightarrow 6a_2'$	yes	3.34[a]	2.76	3.37
$Ru_3(CO)_{12}$	$10a_1' \rightarrow 16e'$	yes	3.89[a]	3.05	3.87
$Ru_3(CO)_{12}$	$14e' \rightarrow 6a_2'$	yes		3.73	4.24
$Os_3(CO)_{12}$	$10a_1' \rightarrow 6a_2'$	no		2.79	not obsd
$Os_3(CO)_{12}$	$15e' \rightarrow 6a_2'$	yes		2.96[a]	3.25 or 3.91
$Os_3(CO)_{12}$	$10a_1' \rightarrow 16e'$	yes		2.97	3.25 or 3.91
$Os_3(CO)_{12}$	$14e' \rightarrow 6a_2'$	yes		3.78	4.51

[a] These energies were calculated with use of the spin-restricted transition-state procedure. All other calculated energies assumed a similar relaxation. Because the relaxation shifts were only 0.05–0.1 eV, the latter assumption will introduce little error. [b] Energies from low-temperature electronic spectra are reported in ref 11.

Electronic and Resonance Raman Spectra and the Excited States. In both $Ru_3(CO)_{12}$ and $Os_3(CO)_{12}$, the dipole-forbidden $10a_1' \rightarrow 6a_2'$ transition is calculated to lie lowest in energy, closely followed by the allowed electronic transitions $15e' \rightarrow 6a_2'$ and $10a_1' \rightarrow 16e'$. Calculated energies for these electronic transitions are listed in Table III, along with their respective peaks in the experimetal spectra. As frequently found for spin-restricted calculations,[38a] the calculated energies underestimate the experimental values; however, for $Ru_3(CO)_{12}$ the relative energies are acceptable. For $Os_3(CO)_{12}$ the two allowed transitions are predicted to be accidently degenerate. Although this conflicts with the experimental data, the trend may be correct. Spectroscopic studies[11] of $Ru_3(CO)_{12}$ and $Os_3(CO)_{12}$ have suggested an *inversion* in the ordering of the two lowest allowed electronic transitions in the latter complex. As noted previously, multiplet effects (see Experimental Section) may be important for the osmium species. The assignments for the lowest dipole-allowed transition agrees with that of Tyler et al. Our calculations indicate a different ($10a_1' \rightarrow 16e'$) assignment for the second dipole-allowed feature.

Frequently, the nature of the excited states of transition-metal complexes has been analyzed in terms of the properties of virtual orbitals produced by ground-state calculations. In covalent systems like $Ru_3(CO)_{12}$ and $Os_3(CO)_{12}$ simple descriptions like ligand to metal charge transfer or $\sigma \rightarrow \sigma^*$ are of uncertain qualitative significance. Therefore, we monitor bonding changes with difference electron density maps. This procedure required a separate MP calculation for each excited state (now promoting a full electron). Each excited-state total density was then subtracted from the electron density distribution in the ground state. This procedure includes orbital relaxation effects. Positive contours signify regions from which electron density has been depleted in the ground $\rightarrow$ excited-state transition, and negative contours represent where this charge has migrated. Contour levels vary logarithmically.

Of prime concern are the three lowest energy transitions $10a_1' \rightarrow 6a_2'$ ($^1A_1' \rightarrow {}^1A_2'$), $15e' \rightarrow 6a_2'$ ($^1A_1' \rightarrow {}^1E'$) and $10a_1' \rightarrow 16e'$ ($^1A_1' \rightarrow {}^1E'$). Comparing the plots of Figures 7 and

(38) (a) Bagus, P. S.; Bennett, B. I. *Int. J. Quantum Chem.* **1975**, *9*, 143–148. (b) Johnson, C. E.; Trogler, W. C. *J. Am. Chem. Soc.* **1981**, *103*, 6352–6358. (c) Albrecht, A. C. *J. Chem. Phys.* **1961**, *34*, 1476–1482.

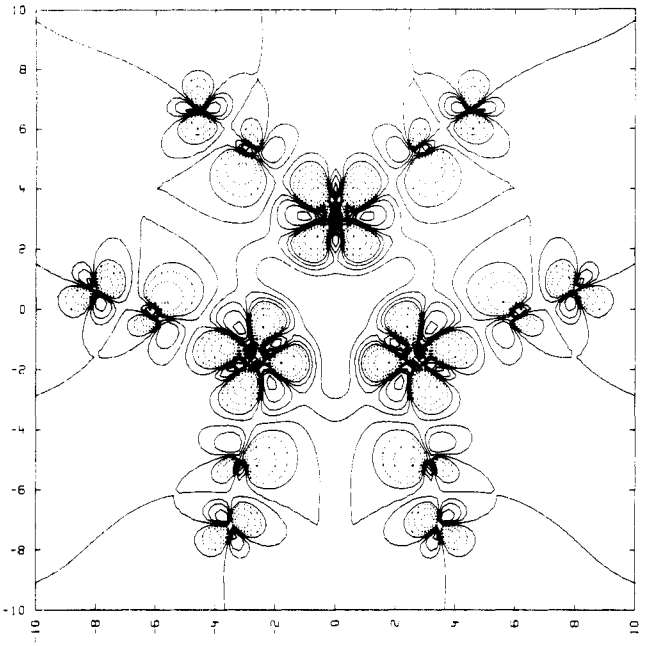

Figure 7. Difference electron density contour plot (ground state minus excited state) for the $10a_1' \rightarrow 6a_2'$ electronic transition in $Ru_3(CO)_{12}$. The lowest (outermost) contours are 0.001 e/a_0^3, and inner contours have double the value of the preceding outer one.

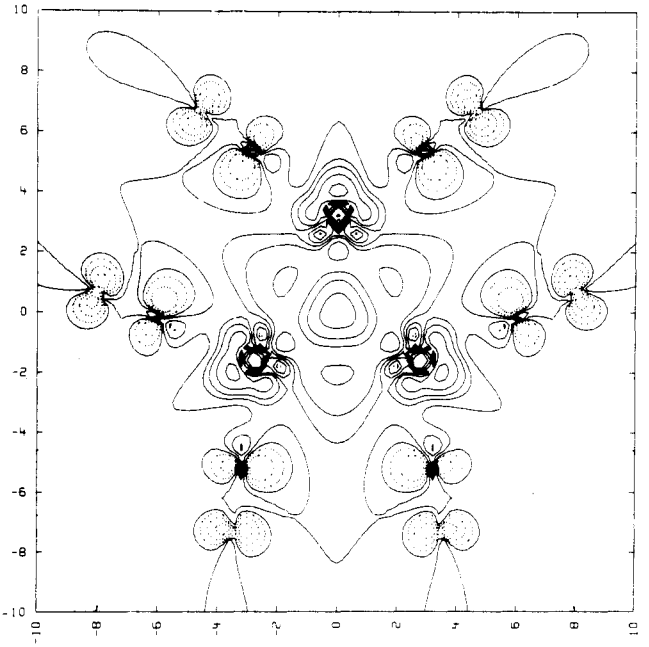

Figure 8. Difference electron density contour plot (ground state minus excited state) for the $15e' \rightarrow 6a_2'$ electronic transition in $Ru_3(CO)_{12}$. Plot parameters are identical with those of Figure 7.

8, we conclude that the $15e' \rightarrow 6a_2'$ excitation leads to a significant decrease of electron density in the metal–metal bonding regions. This weakens the Ru–Ru bonding and helps to rationalize the photofragmentation reactions[17] of these cluster systems (if the nonstatistical approach to reactivity is valid).[38b] The nearly equienergetic HOMO → LUMO ($10a_1' \rightarrow 6a_2'$) (dipole-forbidden) transition does not disrupt Ru–Ru bonding as much, but ruthenium–carbon monoxide bonding changes in this excited state. Note the tilt of electron density in the CO π orbitals *away* from Ru in the excited state, perhaps facilitating Ru–CO dissociative processes. The near degeneracy of the two states helps to rationalize dual aspects (vide supra) of the photochemical reactivity.[17,18] Bonding changes in the $10a_1' \rightarrow 16e'$ excited state possess characteristics

Table IV. Relative Raman Scattering Intensity as a Function of Excitation Wavelength for the Metal–Metal Stretching Vibrations in $Ru_3(CO)_{12}$[a] and $Os_3(CO)_{10}P_2$[b]

	$Ru_3(CO)_{12}$[a]		$Os_3(CO)_{10}P_2$[b]	
excitation wavelength, Å	185 cm^{-1} (0.20)[c]	130 cm^{-1} (0.73)	190 cm^{-1} (0.78)	140 cm^{-1} (0.46)
5145	0.11	0.03	1.00	1.00
5017	0.18	0.08	1.15	1.05
4965	0.15	0.06	1.82	1.95
4880	0.16	0.07	1.95	2.11
4765			2.26	2.37
4658			1.49	1.26
4579	0.32	0.15	1.44	*d*

[a] In dichloromethane solution. [b] In THF solution; P is diphenylneomenthylphosphine. [c] Depolarization ratios given in parentheses; values are ±10%. [d] Peak obscured by plasma line.

common to both the preceding transitions; significant depletion of Ru–Ru bonding electron density as well as the tilting of π-electron density on CO is evident.

Spectroscopic evidence supports these theoretical expectations. Magnetic circular dichroism measurements[11] prove that the two lowest allowed transitions in $Ru_3(CO)_{12}$ and $Os_3(CO)_{12}$ are degenerate ($^1E'$). We have measured resonance Raman spectra on the low-energy side of the first electronic absorption band in $Ru_3(CO)_{12}$. *Both* the 185 (a_1') and 130-cm^{-1} (e') Ru–Ru stretching vibrations exhibit resonance enhancement (Table IV). These vibrations are assigned on the basis of force-field calculations[39] and polarization measurements (Table IV). Typically those vibrational modes that experience Franck–Condon distortions in the excited state exhibit resonance enhancement. The experimental data confirms the prediction of disrupted Ru–Ru bonding in the lowest allowed transition $15e' \rightarrow 6a_2'$. Resonance enhancement of the e' vibration demonstrates an additional Jahn–Teller distortion in the $^1E'$ ($15e' \rightarrow 6a_2'$) excited electronic state or *B*-term scattering[38c] (if $^1E'$ is strongly vibronically coupled with $^1A_2'$). This result may be relevant to photochemical metal–metal bond-cleavage reactions of these clusters. One orthogonal representation of the e' normal mode is provided:

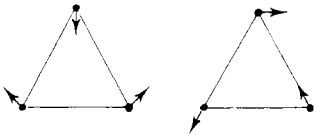

This sketch emphasizes the weakening of a single bond of the trinuclear framework. Linear trimeric complexes have often been postulated as primary photoproducts in these systems.[17,18,22]

Limitations on the available laser frequencies prevented us from obtaining resonance Raman data for $Os_3(CO)_{12}$; however, spectra have been measured for $Os_3(CO)_{10}[P(C_6H_5)_2(C_{10}H_{19})]_2$ [λ_{max} (ϵ) 430 nm (7200), 364 nm (9700), 321 nm (sh), 261 nm (24 700)]. This complex absorbs at lower energies than $Os_3(CO)_{12}$, and its resonance Raman behavior is described in Table IV. The low-energy shoulder on the first electronic absorption band system again displays resonance enhancement of two vibrations in the Os–Os stretching region (e.g., in $Os_3(CO)_{12}$: a_1' at 158 cm^{-1} and e' at 117 cm^{-1}). Although the 140-cm^{-1} peak appears similar to the 158-cm^{-1} (a_1') vibration of $Os_3(CO)_{12}$, the 190-cm^{-1} vibration cannot be unambiguously assigned. Again, the lowest allowed transition provides evidence for significant distortion of metal–metal bonding. These results concur with the earlier hypothesis[11] that phosphine substitution results in a bathochromic shift of in-plane (metal) bonding to antibonding transitions.

(39) Quicksall, C. O.; Spiro, T. G. *Inorg. Chem.* **1968**, *7*, 2365–2369.

Cluster Basicity. In strongly acidic media Davidson et al.[40] discovered that metal carbonyl compounds can undergo protonation. Later, infrared and ^1H NMR data were reported for $HOs_3(CO)_{12}^+$, $HRu_3(CO)_{12}^+$, $H_2Ir_4(CO)_{12}^{2+}$, and a variety of $H_2Os_3(CO)_{12-x}(L)_x^{2+}$ complexes.[41,42] All of these compounds were prepared by dissolution in 98% H_2SO_4. Knight and Mays[42] reported infrared data for $Ru_3(CO)_{12}$ and $Os_3(CO)_{12}$ in neat trifluoroacetic acid. Although they did not assign them as such it is apparent that the species present are the protonated clusters. Subsequent solution NMR studies[41] and inelastic neutron-scattering experiments[43] supported edge protonation in $[HRu_3(CO)_{12}]^+$ and $[HOs_3(CO)_{12}]^+$. The miscibility of trifluoroacetic acid with organic solvents allowed us to titrate (Supplementary Figure 1) the trinuclear clusters to the monoprotonated species in CH_2Cl_2 solution. The protonated osmium complex exhibits absorptions with λ_{max} (ϵ) 369 (8800), 305 (6400), and 275 nm (sh). Bands at λ_{max} (ϵ) 400 (1100), 345 (sh), 286 (sh), and 270 nm (8100) characterize the ruthenium analogue. Protonation blue shifts the spectra and leaves one low-energy transition. Recall that the plot for the $10a_1' \rightarrow 6a_2'$ transition showed little change in the electron density along the edge of the Ru_3 cluster. Provided that orbital hybridization does not change greatly, this transition's energy would only slightly vary upon edge protonation. Lowering the symmetry now provides electric dipole intensity. From spectrophotometric titrations,[44] the osmium cluster appears to be 5 times more basic than the ruthenium analogue. A similarity in the proton-acceptor ability of $Ru_3(CO)_{12}$ and $Os_3(CO)_{12}$ conforms with their similar first IP's, net d-electron populations, and orbital splittings.

Acknowledgment. We thank the National Resource for Computation in Chemistry for a grant of computer time. This work was supported in part by the National Science Foundation, Grant DMR79-25379. Work performed at ANL was done under the auspices of the Division of Basic Energy Sciences of the U.S. Department of Energy. Professor Duward Shriver generously provided us access to his Raman spectrometer.

Registry No. $Ru_3(CO)_{12}$, 15243-33-1; $Os_3(CO)_{12}$, 15696-40-9.

Supplementary Material Available: Tables of orbital energies for the SCC-DV-Xα calculations of $Os_3(CO)_{12}$ and $Ru_3(CO)_{12}$ and the MP-DV-Xα calculation of $Os_3(CO)_{12}$, IP's from all four calculations, and atomic populations from the four calculations and a figure of the titration of $Os_3(CO)_{12}$ with HO_2CCF_3 in CH_2Cl_2 (4 pages). Ordering information is given on any current masthead page.

(40) Davidson, A.; McFarlane, W.; Pratt, L.; Wilkinson, G. *J. Chem. Soc.* **1962**, 3653.
(41) Deeming, A. J.; Johnson, B. F. G.; Lewis, J. *J. Chem. Soc. A* **1970**, 2967-2971. Koridze, A. A.; Kizas, O. A.; Astakhova, N. M.; Petrovskii, P. V.; Grishin, Y. K. *J. Chem. Soc., Chem. Commun.* **1981**, 853-855.
(42) Knight, J.; Mays, M. J. *J. Chem. Soc. A* **1970**, 711-714.
(43) White, J. W.; Wright, W. *J. Chem. Soc. A* **1971**, 2843-2847.
(44) Hammett, L. P. "Physical Organic Chemistry"; McGraw-Hill: New York, 1970.

Contribution from the Institut für Anorganische, Analytische und Physikalische Chemie der Universität Bern, CH-3000 Bern 9, Switzerland

Low-Temperature Structural and Spectroscopic Properties of $[Cr_3O(CH_3COO)_6(H_2O)_3]Cl \cdot 6H_2O$

KURT J. SCHENK and HANS U. GÜDEL*

Received November 3, 1981

The structural properties of the title compound were studied by X-ray diffraction at 190 K. The compound undergoes a structural phase transition at 211 K. HT and LT space groups are $P2_12_12$ and $P2_12_12_1$, respectively. The LT unit cell is twice as long in the *c* direction as the HT cell, with *a* and *b* unchanged. In the LT structure, there are two inequivalent sets a and b of triangular clusters. Measurements of the luminescence spectra, decay curves, and time-resolved spectra in the temperature range 7-83 K revealed that there is no excitation energy transfer (ET) between clusters at 7 K. With increasing temperature, ET sets in; and an upper limit estimate for the transfer rate from set a to b clusters at 83 K is 9×10^4 s^{-1}. A value of 0.1 cm^{-1} is obtained as an upper limit estimate for the intercluster exchange parameter. The LT magnetic and spectroscopic properties result from geometrical distortions of triangular clusters.

1. Introduction

The chloride salt of basic chromium(III) acetate (abbreviated CRAC in the following) has been the subject of a large number of experimental and theoretical studies. The principal aim of the majority of those investigations was an understanding of the exchange effects responsible for the unusual low-temperature (LT) thermal and magnetic properties. In a recent article by Brown and co-workers, the earlier work in this area was briefly reviewed.[1]

At room temperature the chromium(III) ions of the trimeric complexes form equilateral triangles within the rather low accuracy of the crystal structure determination.[2] The clusters are well separated and insulated from one another by the bulky ligands and the highly disordered water/anion structure. The shortest intercluster Cr-Cr distance is 5.78 Å, as compared to 3.27 Å within the trimers. At 211 K CRAC undergoes a first-order structural phase transition.[3] Whereas all the trimeric complexes are crystallographically equivalent in the high-temperature (HT) phase, there are two sets of inequivalent complexes in the LT phase.[4]

A very detailed and accurate description of exchange splittings in both sets a and b of clusters was obtained from absorption and luminescence spectra.[4] On the basis of a model originally proposed by Sorai and co-workers[3] to rationalize the LT heat capacity of CRAC, the observed electronic splittings were interpreted as resulting from geometrically distorted triangular complexes.[4] Since there was no direct experimental evidence for the existence of distorted complexes in the LT

(1) Wrobleski, J. T.; Dziobkowski, C. T.; Brown, D. B. *Inorg. Chem.* **1981**, *20*, 684.
(2) Chang, S. C.; Jeffrey, G. A. *Acta Crystallogr., Sect. B* **1970**, *B26*, 673.
(3) Sorai, M.; Tachiki, M.; Suga, H.; Seki, S. *J. Phys. Soc. Jpn.* **1971**, *30*, 750.
(4) Ferguson, J.; Güdel, H. U. *Chem. Phys. Lett.* **1972**, *17*, 547.

0020-1669/82/1321-2253$01.25/0